

# Visualization of the Hartree-Fock ground state of the two-dimensional Hubbard model

Kazue Matsuyama and Jeff Greensite  
 Physics and Astronomy Department  
 San Francisco State University  
 San Francisco, CA 94132, USA  
 (Dated: January 19, 2022)

We explore certain properties of the Hartree-Fock approximation to the ground state of the two-dimensional Hubbard model, emphasizing the fact that in the Hartree approach there is an enormous multiplicity of self-consistent solutions which are nearly degenerate in energy, reminiscent of a spin glass, but which may differ substantially in other bulk properties. In this framework we compute various observables, and find that some regions of the phase diagram exhibit patterns which include not only stripes but also other types of periodicity, and that different self-consistent solutions, at the same set of parameters, may be associated with different types of patterns. We find pair correlation near half-filling, association of magnetic order with an energy gap, and also, at strong repulsion ( $U/t \gg 1$ ), localization of either particle or hole states, depending on the filling fraction.

## I. INTRODUCTION

The essence of the Hartree-Fock approach to many-electron systems is to effectively replace the problem of diagonalizing the many body Hamiltonian with the problem of diagonalizing a one-electron Hamiltonian, with a potential term to be computed self-consistently. The application of this idea to the Hubbard model dates at least to ref. [1], and there have been very many refinements since then, see e.g. [2–12] and references therein. Our mean field approximation to the Hubbard Hamiltonian is fairly standard, but we emphasize in particular: (i) the enormous multiplicity of self-consistent ground states, suggestive of a spin glass; (ii) the emergence of different types of geometric order in spin/charge distributions at the same point in phase space; (iii) the absence of any particle localization associated with geometric ordering; (iv) the appearance of either particle or hole localization at very strong repulsion on either side of half-filling; and (v) the occurrence of pairing, with some of the characteristics of d-wave order, in the immediate neighborhood of half-filling.

We motivate the mean field approximation to the Hubbard Hamiltonian as follows. Let us suppose that we have  $M$  electrons on a two dimensional  $L \times L$  square lattice with periodic boundary conditions, interacting according to the usual Hubbard model Hamiltonian

$$H = -t \sum_{\langle xy \rangle} \sum_{s=\uparrow, \downarrow} c^\dagger(x, s) c(y, s) + U \sum_x c^\dagger(x, \uparrow) c(x, \uparrow) c^\dagger(x, \downarrow) c(x, \downarrow), \quad (1)$$

with the first term a sum over nearest neighbors, and define the Hartree-Fock state  $|\Phi\rangle = \Phi|0\rangle$  where

$$\Phi = \prod_{i=1}^M \sum_{\mathbf{x}_i} \phi_i(\mathbf{x}_i) c^\dagger(\mathbf{x}_i), \quad (2)$$

and where the single-particle states  $\{\phi_i\}$  are all orthogonal. Our notation is that  $\mathbf{x} = (x, s)$  where  $x$  labels the lattice site,

and  $s = \{\uparrow, \downarrow\}$  is the spin. Now we introduce an operator for an auxiliary (and fictitious) electron interacting with the other  $M$  electrons, and define the reduced one-particle Hamiltonian  $H[\Phi]$  with matrix elements

$$H_{\mathbf{w}_1, \mathbf{w}_2}[\Phi] = \langle 0 | \Phi^\dagger c(\mathbf{w}_1) H c^\dagger(\mathbf{w}_2) \Phi | 0 \rangle_{conn}, \quad (3)$$

where the subscript *conn* means that we keep only contributions to the expectation value which contain the anticommutators of  $c(\mathbf{w}_1)$  and  $c^\dagger(\mathbf{w}_2)$  with creation/destruction operators in  $H$ . This is our candidate for the Hamiltonian describing the propagation of a single electron in the average field of all other electrons. The approximation to the Hubbard model ground state is arrived at by an iterative procedure. Given  $\Phi^{(n)}$  at the  $n$ -th iteration, we solve numerically the eigenvalue problem

$$H[\Phi^{(n)}] \phi_i(\mathbf{x}) = \varepsilon_i \phi_i(\mathbf{x}) \quad (4)$$

for the  $M$  lowest energy states, and insert those eigenstates  $\{\phi_i, i = 1, 2, \dots, M\}$  into (2) to obtain the next approximation  $|\Phi^{(n+1)}\rangle$  to the ground state at the  $(n+1)$ -th iteration. The procedure terminates when a certain convergence criterion, described below, is satisfied.

## II. PROCEDURE

It is straightforward, given  $\Phi$ , to find the non-zero matrix elements:

$w_1, w_2$  nearest neighbors

$$H[\Phi]_{\mathbf{w}_1, \mathbf{w}_2} = -t \delta_{s_1, s_2} \quad (5)$$

$w_1 = w_2 = w$  same site

$$\begin{aligned}
H[\Phi]_{w\uparrow,w\uparrow} &= U\rho(w,\downarrow,\downarrow) \\
H[\Phi]_{w\downarrow,w\downarrow} &= U\rho(w,\uparrow,\uparrow) \\
H[\Phi]_{w\uparrow,w\downarrow} &= -U\rho(w,\downarrow,\uparrow) \\
H[\Phi]_{w\downarrow,w\uparrow} &= -U\rho(w,\uparrow,\downarrow).
\end{aligned} \tag{6}$$

where

$$\begin{aligned}
\rho(w,\downarrow,\downarrow) &= \sum_{i=1}^M \phi_i^*(w,\downarrow)\phi_i(w,\downarrow) \\
\rho(w,\uparrow,\uparrow) &= \sum_{i=1}^M \phi_i^*(w,\uparrow)\phi_i(w,\uparrow) \\
\rho(w,\downarrow,\uparrow) &= \sum_{i=1}^M \phi_i^*(w,\downarrow)\phi_i(w,\uparrow) \\
\rho(w,\uparrow,\downarrow) &= \sum_{i=1}^M \phi_i^*(w,\uparrow)\phi_i(w,\downarrow).
\end{aligned} \tag{7}$$

The problem is then to find the eigenvalues and corresponding eigenvectors of a  $2L^2 \times 2L^2$  sparse matrix, which can be handled by standard numerical software.<sup>1</sup> It is important to point out here that the iterative procedure does not converge to a unique ground state, but depends instead on the (random) initialization. Energy densities are only very weakly dependent on the initialization; magnetization and spatial distributions have a far stronger dependence; we will return to this point below. We initialize the system with a small, random choice of  $\rho$ , i.e. at each site  $w$  we generate three uniformly distributed random numbers  $r_1, r_2, r_3$  in the range  $[0, 1]$ , and let

$$\begin{aligned}
\rho(w,\uparrow,\uparrow) &= ar_1 \\
\rho(w,\downarrow,\downarrow) &= ar_2 \\
\rho(w,\uparrow,\downarrow) &= \rho(w,\downarrow,\uparrow) = b(r_3 - 0.5),
\end{aligned} \tag{8}$$

with  $a, b$  taken to be small constants, e.g.  $a = 0.01, b = 0.001$ . The choice, and even the order of magnitude of these constants is not critical. However, while each set of iterations converges to a solution with very nearly degenerate energy densities, typically differing by fractional deviations of order  $O(10^{-4})$ , solutions obtained with different stochastic starting points vary widely in the spatial distribution of spin up and spin down electron densities. If this Hartree-Fock result reflects a true property of the 2D Hubbard model, then the enormous multiplicity of nearly degenerate ground states is reminiscent of a spin glass.

After the first iteration, one usually finds equal numbers of electrons of either spin

$$\sum_w \rho(w,\uparrow,\uparrow) = \sum_w \rho(w,\downarrow,\downarrow) = \frac{1}{2}M, \tag{9}$$

but any small deviation from this sum rule is corrected by adding or subtracting a small constant of order  $1/L^2$  to the

electron densities, prior to the next iteration. Thus we are selecting for self-consistent solutions with equal numbers of up and down spins. The convergence criterion is that after  $n$  iterations the mean square deviations of electron spin densities satisfy

$$\begin{aligned}
\frac{1}{L^2} \sum_w (\rho^{(n)}(w,\uparrow,\uparrow) - \rho^{(n-9)}(w,\uparrow,\uparrow))^2 &< \delta^2 \\
\frac{1}{L^2} \sum_w (\rho^{(n)}(w,\downarrow,\downarrow) - \rho^{(n-9)}(w,\downarrow,\downarrow))^2 &< \delta^2,
\end{aligned} \tag{10}$$

where the  $\rho^{(n)}$  denote densities obtained after the  $n$ -th iteration. We choose  $\delta = 0.001$ .

In all our numerical computations we have taken  $t = 1$ , so  $U/t = U$  in the results reported below.

### A. Relation to the mean field decomposition

With the subtraction of an (irrelevant) constant, the operator

$$H_{mf} = \sum_{\mathbf{w}_1, \mathbf{w}_2} c^\dagger(\mathbf{w}_1) H[\Phi]_{\mathbf{w}_1, \mathbf{w}_2} c(\mathbf{w}_2) - E_0 \tag{11}$$

is the standard mean field approximation to the Hubbard model Hamiltonian, where

$$E_0 = U \sum_x (\rho(x,\uparrow,\uparrow)\rho(x,\downarrow,\downarrow) - \rho(x,\uparrow,\downarrow)\rho(x,\downarrow,\uparrow)), \tag{12}$$

cf. Fazekas [9], and Lechermann in [13]. Some authors, however, adopt a simpler mean-field decomposition. Writing

$$n(x,\uparrow)n(x,\downarrow) = c^\dagger(x,\uparrow)c(x,\uparrow)c^\dagger(x,\downarrow)c(x,\downarrow), \tag{13}$$

where

$$n(x,s) = c^\dagger(x,s)c(x,s), \tag{14}$$

the simpler decomposition is

$$\begin{aligned}
&c^\dagger(x,\uparrow)c(x,\uparrow)c^\dagger(x,\downarrow)c(x,\downarrow) \\
&\rightarrow n(x,\uparrow)\langle n(x,\downarrow) \rangle + \langle n(x,\uparrow) \rangle n(x,\downarrow) - \langle n(x,\uparrow) \rangle \langle n(x,\downarrow) \rangle,
\end{aligned} \tag{15}$$

and in our notation this amounts to dropping the spin-flip terms  $H[\Phi]_{x\uparrow,x\downarrow}$  and  $H[\Phi]_{x\downarrow,x\uparrow}$  in  $H_{mf}$ . This is what is done in the Hartree-Fock calculations of ref. [10], whose approach is in other respects quite similar to our own. Dropping the spin-flip terms means that ground state can be expressed as antisymmetrized products of one particle wave functions of definite spin. On the other hand it is a severe truncation of the mean field expansion discussed, e.g., in [9] and, as remarked in [13], it is a little like keeping the Hartree term but dropping the Fock term. We prefer not to drop these spin flip terms, which means that every one particle wave function  $\phi_i(x,s)$  has an amplitude for every position  $x$  and each spin  $s = \uparrow, \downarrow$ .

<sup>1</sup> We use the Matlab `eigs` function.

### III. OBSERVABLES

Once a self-consistent solution is obtained, we compute:

- The energy density

$$\mathcal{E} = \frac{1}{L^2} \sum_{i=1}^M \varepsilon_i . \quad (16)$$

- The energy gap (at zero temperature) between the highest energy occupied and next unoccupied states

$$\Delta\varepsilon = \varepsilon_{M+1} - \varepsilon_M . \quad (17)$$

- Charge and spin densities

$$\begin{aligned} C(x) &= \rho(x, \uparrow, \uparrow) + \rho(x, \downarrow, \downarrow) \\ D(x) &= \rho(x, \uparrow, \uparrow) - \rho(x, \downarrow, \downarrow) . \end{aligned} \quad (18)$$

- Local magnetization

$$m = \frac{1}{2L^2} \sum_x \sum_{\mu=1}^2 D(x) D(x + \hat{\mu}) . \quad (19)$$

- Long range order. In principle any regular arrangement of spins in the 2D Hubbard model, at any non-zero temperature, is a violation of the Mermin-Wagner theorem. Nevertheless, such arrangements have been observed on finite lattices in quantum Monte Carlo simulations at half-filling [14]; this must be attributed to the very low (zero) temperature and finite volume. A useful observable to probe periodicity, at least on the scale of the finite lattice, is

$$\begin{aligned} S(k) &= \frac{1}{L^2} \sum_{x,y} D(x) D(y) e^{ik \cdot (x-y)} \\ &= \frac{1}{L^2} \tilde{D}(k) \tilde{D}^*(k) , \end{aligned} \quad (20)$$

where  $\tilde{D}(k)$  is the Fourier transform of the spatial spin distribution  $D(x)$ . We have long range order (with the caveat just mentioned), when  $S(k)$  is concentrated at only a few values of  $k$ , typically resulting in either a checkerboard, stripe, or rectangular domain pattern.

- Localization. We can judge whether individual energy eigenstates  $\phi_i(x, s)$  are localized by computing the inverse participation ratio (IPR)

$$IPR_i = \sum_x \sum_s (\phi_i^*(x, s) \phi_i(x, s))^2 , \quad (21)$$

where  $IPR = 1$  means that the electron is localized to a single site, and  $IPR \approx 1/L^2$  indicates that the positional probability density is spread evenly over the lattice area.

- Momentum distribution. We compute momentum-space occupation numbers

$$\begin{aligned} n(k) &= \frac{1}{2L^2} \sum_{x,y,s} e^{ik \cdot (x-y)} \langle \Phi | c^\dagger(x, s) c(y, s) | \Phi \rangle \\ &= \frac{1}{2L^2} \sum_{i,s} \phi_i^*(k, s) \phi_i(k, s) , \end{aligned} \quad (22)$$

where

$$\phi_i(k, s) = \sum_x e^{ik \cdot x} \phi_i(x, s) , \quad (23)$$

and we also compute the magnitude of the discretized gradient

$$\begin{aligned} \nabla_x n(k) &= \frac{L}{4\pi} (n(k_x + 1, k_y) - n(k_x - 1, k_y)) \\ \nabla_y n(k) &= \frac{L}{4\pi} (n(k_x, k_y + 1) - n(k_x, k_y - 1)) \\ |\nabla n(k)| &= \sqrt{(\nabla_x n)^2 + (\nabla_y n)^2} . \end{aligned} \quad (24)$$

- Pairing correlations. We search for d-wave arrangements in the correlator

$$\Delta(k', k) = \langle c^\dagger(k', \uparrow) c^\dagger(-k', \downarrow) c(k, \uparrow) c(-k, \downarrow) \rangle , \quad (25)$$

where  $k' \neq k$ , and choosing the  $x, y$  components of  $k$  to be the  $y, x$  components of  $k'$ .

## IV. RESULTS

### A. Momentum space distributions

A good starting point is to compare our results for momentum space distributions  $n(k)$  and gradients  $|\nabla n(k)|$  with the results of Monte Carlo simulations, particularly where those Monte Carlo results exist away from half-filling. Because of the sign problem, Monte Carlo simulations away from half-filling must rely on a reweighting procedure of some kind [15], and this apparently does not work down to zero temperature. Thus our comparison with the Monte Carlo simulations of Varney et. al [14], away from half-filling, is necessarily a comparison of our zero temperature results with Monte Carlo simulations at finite temperature. The comparison is nonetheless interesting, even if only at the qualitative level.

In Fig. 1 we display our results (on a  $24^2$  lattice) for momentum distributions  $n(k)$  and gradients  $|\nabla n(k)|$  at the same densities  $f = 0.23, 0.41, 0.61, 0.79, 1.0$  used in ref. [14], and Fig. 1 should be compared with Fig. 2 in that reference (we will also refer to density  $f$  as the ‘‘filling fraction’’, with the understanding that  $f = 1$  refers to half-filling). Despite the finite temperatures used in [14] the figures are very similar, even at the quantitative level. Note in particular the blurring of the boundary between occupied and unoccupied states, at the larger filling fractions, as  $U$  is increased from  $U = 2$  to

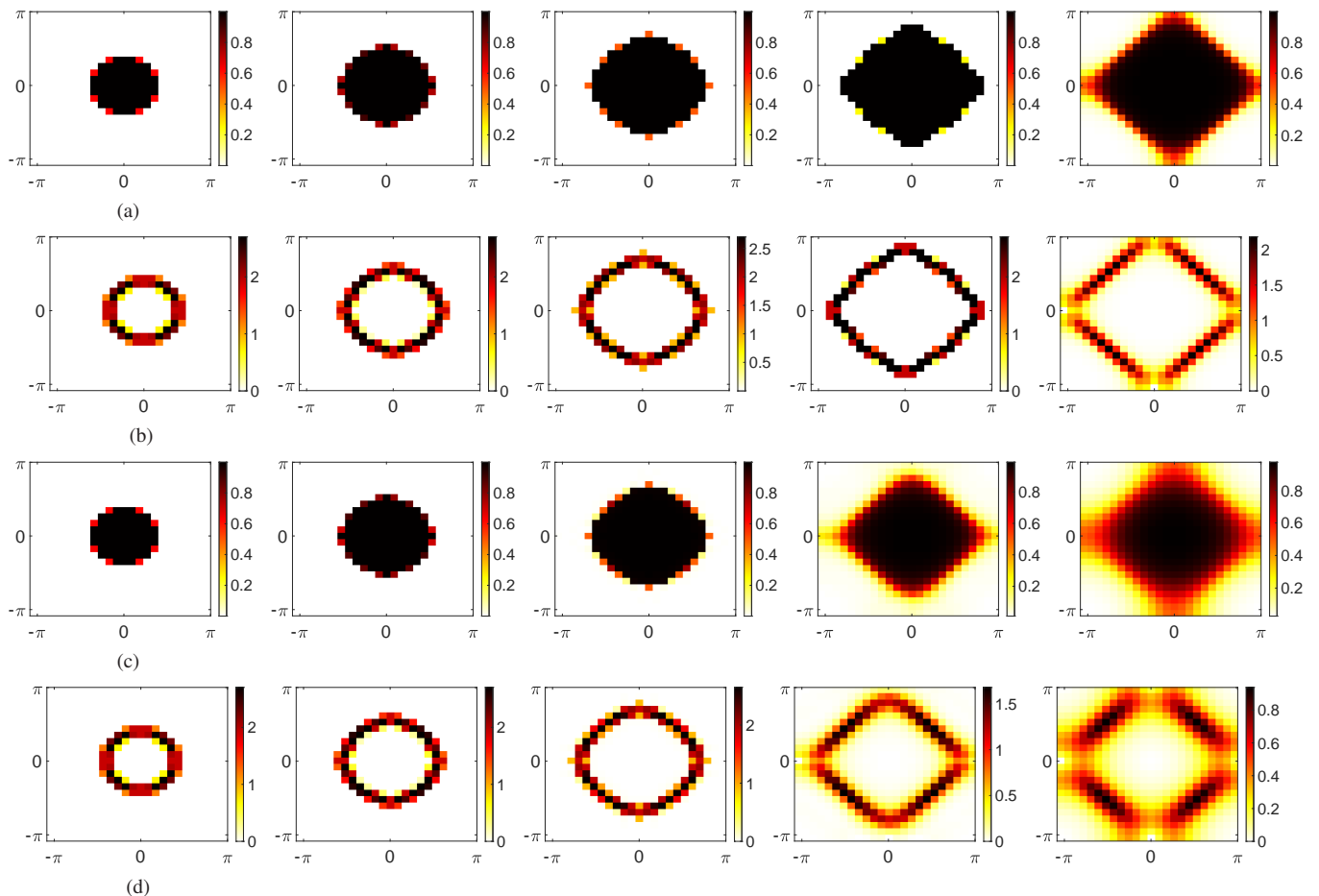


FIG. 1. 2D color plots of the momentum distribution  $n(k_x, k_y)$  and the magnitude  $|\nabla n|$  of its gradient. This plot should be compared with the Monte Carlo results displayed in Figure 2 of Varney et al. [14]. Filling fractions, increasing horizontally from left to right, are  $f = 0.23, 0.41, 0.61, 0.79, 1.0$ , where  $f$  is the filling fraction. (a)  $n(k)$  at  $U/t = 2$ ; (b)  $|\nabla n|$  at  $U/t = 2$ ; (c)  $n(k)$  at  $U/t = 4$ ; (d)  $|\nabla n|$  at  $U/t = 4$ .

$U = 4$ .

### B. Multiplicity of self-consistent states

One significant aspect of the Hartree-Fock approach to the 2D Hubbard model is that there is no unique self-consistent solution for the ground state. Instead there are very many such states, obtained from different random starts (8), except, of course, at  $U = 0$ . In Fig. 2 we show our results at filling fraction  $f = 0.8$  on  $24^2$  lattices for the energy density  $\varepsilon$ , the local magnetization  $m$ , and the energy gap  $\Delta\varepsilon$ , together with their standard deviations. The standard deviations are obtained at each  $U$  from 20 separate self-consistent states, obtained as described in section II. These are plotted in Fig. 2 as error bars, but we stress that in these figures the “error bar” represents the standard deviation, rather than standard deviations of the mean.

The standard deviation of energy density,  $\sigma_\varepsilon$ , is so small that it is not discernible in Fig. 2(a). As in a spin glass, with a landscape of local minima of near-degenerate energies, the different self-consistent solutions are nearly degenerate in en-

ergy. The difference between these self-consistent states is quite apparent, however, in the local magnetization  $m$  and the energy gap  $\Delta\varepsilon$ , seen in Figs. 2(b) and 2(c) respectively. In these cases, at  $f = 0.8$  and  $U \geq 3$  (where local antiferromagnetic order becomes apparent), the standard deviations are quite substantial, indicating that despite their near-degeneracy in energy, these different self-consistent solutions are physically distinct.

### C. Local magnetization and the energy gap

In general there is a correlation, at zero temperature, between local magnetization  $m$  and the gap  $\Delta\varepsilon$  between the energies of the last occupied and first unoccupied states. These gaps increase with  $|m|$ , which in turn is largest at or near half-filling, and large  $U$ . In Fig. 3(a) we display a histogram of energies  $\varepsilon_n$  vs.  $n$  on a  $24 \times 24$  lattice at  $U = 4$  and filling fraction  $f = 0.9$ , taken from a typical configuration which has converged from a random initialization, as described above. This is a closeup view of energies in neighborhood of  $n = M$ , with the energy of the last occupied state ( $n = M = 518$  for these

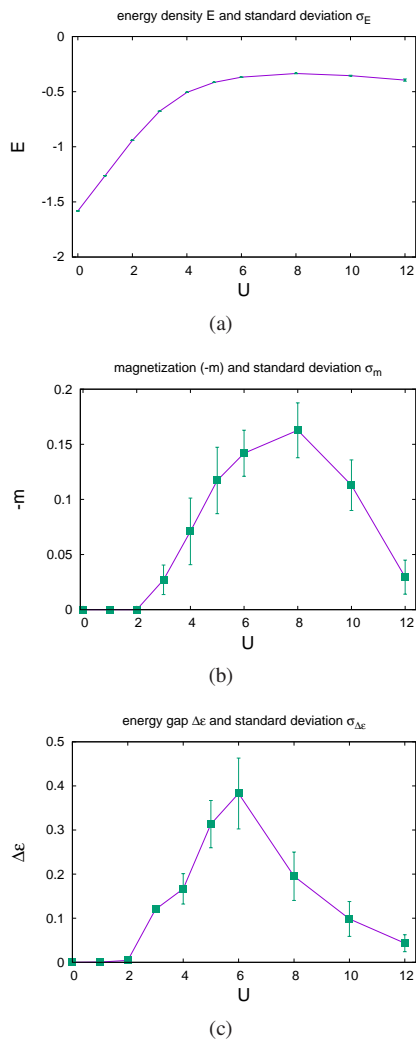


FIG. 2. Values and standard deviations vs.  $U$  at filling fraction  $f = 0.8$  of (a) energy density  $\mathcal{E}$ ; (b) local magnetization  $m$ ; and (c) energy gap  $\Delta\mathcal{E}$ . Standard deviations, displayed as error bars, were taken from a set of twenty independent, self-consistent Hartree-Fock solutions. Note that no deviation is visible among these different solutions in the energy density, but there are significant deviations in the magnetization and energy gap for  $U \geq 3$ .

parameters) shown in a different color. Note the significant jump in energy between the last occupied state and the first unoccupied state ( $n = M + 1$ ). Figure 3(b) is a more global display of the energies, beginning at the lowest energy.

At moderate values of  $U$ , in a region centered around half-filling ( $f = 1$ ), we find that the local magnetization defined in (19) is significantly non-zero and negative, indicating local antiferromagnetism. It is interesting that the local magnetization is closely correlated with the existence of an energy gap  $\Delta\mathcal{E} > 0$ . And example of this correlation, at  $U = 4$  on a  $24^2$  lattice, is shown in Fig. 4. In order that both the magnetization and energy gap are clearly visible on the same figure, we have multiplied the magnetization by a factor of  $-4$ .

A more complete picture of the local magnetization  $m$  and

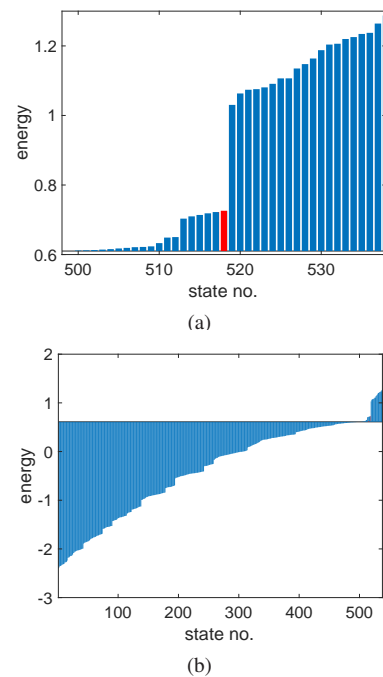


FIG. 3. A histogram of energy vs. state number, with the bar for the last occupied state  $\mathcal{E}_M$  shown in red.  $U = 4, f = 0.9$  on a  $24^2$  lattice. (a) A closeup of energies in the region of the last occupied state; here the gap to the first unoccupied state is quite clear. (b) Overview of energies  $\epsilon_i$  up to, and a little beyond, the last occupied state.

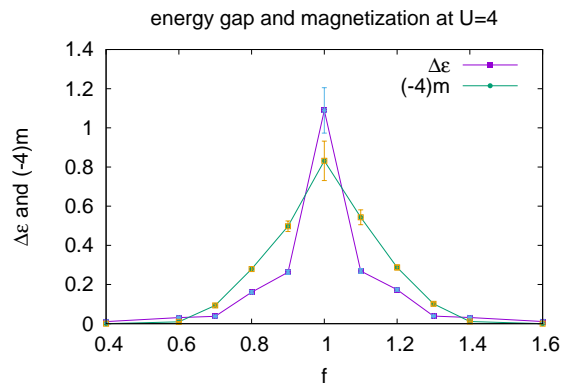
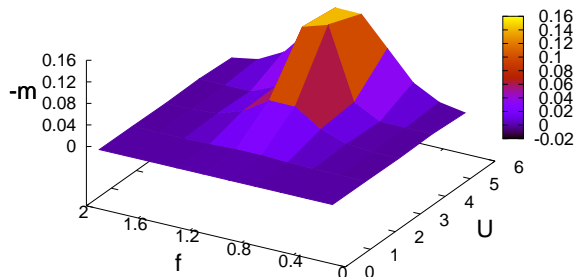
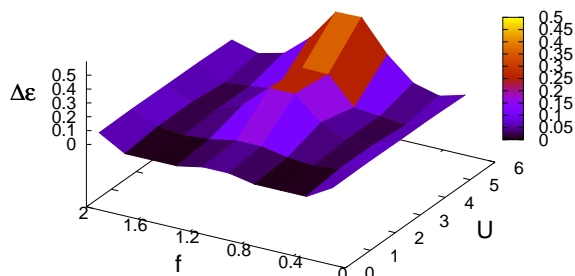
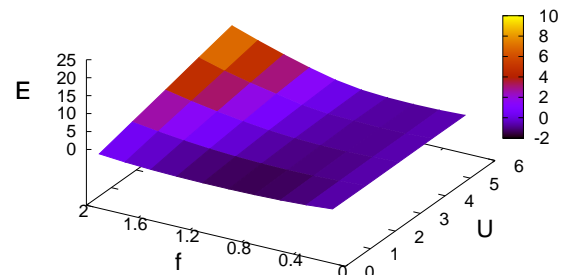


FIG. 4. Energy density and magnetization vs. filling fraction  $f$  at  $U = 4$  on a  $24^2$  lattice. In this plot we have multiplied the magnetization by  $-4$ , for ease of comparison.

energy gap  $\Delta\mathcal{E}$  in the  $U - f$  parameter plane up to  $U = 6$  is shown in Figs. 5(a) and 5(b). Again we see that local antiferromagnetic order in some region of the phase diagram is correlated with the existence of an energy gap  $\Delta\mathcal{E}$ . The energy density in the  $U - f$  plane is shown in Fig. 5(c). There is no obvious indication in this figure of any non-analyticity indicating a thermodynamic phase transition, although other types of phase transitions (see, e.g., [16]) may exist. We note in passing that the energy density at  $U = 0$  is symmetric around half-filling, as can be verified analytically.

(a)  $(-1) \times$  local magnetization

(b) energy gap



(c) energy density

FIG. 5. Surface plots of (a) local magnetization  $\times(-1)m$ ; (b) energy gap  $\Delta\epsilon$ ; (c) energy density  $\mathcal{E}$ ; vs. coupling  $U$  and filling fraction  $f$ . All data taken on  $30^2$  lattices. Note, in (a,b), that the region of significant local antiferromagnetic order is also the region where the energy gap is significant.

Fig. 6 is a 2D color plot of the local magnetization in the  $f-U$  plane up to  $U = 12$ . Data is taken from the average of results obtained from 20 independent Hartree-Fock ground state solutions on a  $30^2$  lattice. The brightly colored oval region is a region of local antiferromagnetism; the local magnetization is negligible outside this region. At the upper border

of the diagram, at  $U = 12$ , the local magnetization turns positive away from half-filling, e.g. at  $f = 0.7, 1.3$  which marks the beginning of ferromagnetic regions in the phase diagram. In Fig. 7 we plot magnetization vs.  $U$  at fixed  $f = 0.7$ , also averaging results taken from 20 solutions on a  $30^2$  lattice (again with “error bars” representing standard deviations) and it is clear that at this filling fraction, from  $U = 11$  onwards, the local magnetization is ferromagnetic rather than antiferromagnetic. All in all, the picture is consistent, at least qualitatively, with much earlier Hartree-Fock explorations of the 2D Hubbard model, e.g. [2]

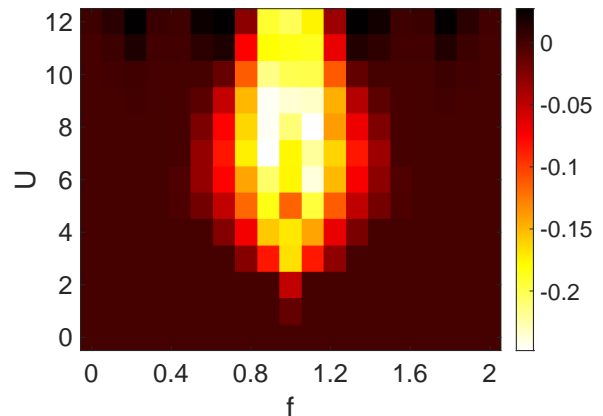


FIG. 6. Color plot of local magnetization  $m$  in the  $f-U$  plane up to  $U = 12$ . The bright region is a region of local antiferromagnetism, surrounded by a region of negligible magnetization.

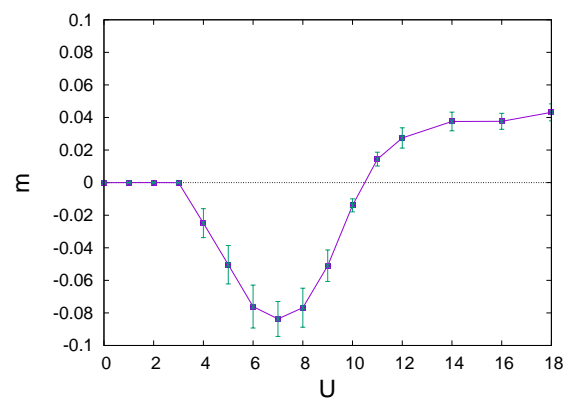


FIG. 7. Local magnetization  $m$  vs.  $U$  at fixed filling fraction  $f = 0.7$ . We note that the local magnetization switches from antiferromagnetic to ferromagnetic around  $U = 11$ . The “error bars” shown actually represent the standard deviation taken from 20 independent, self consistent Hartree-Fock solutions.

### 1. Large $U$ limit

At  $U = 0$  the energies of one-particle states can be computed analytically,

$$\varepsilon(m, n) = -2(\cos(2\pi n/L) + \cos(2\pi m/L))$$

where  $m, n = 0, 1, \dots, L-1$ , (26)

and, after sorting these values from lowest to highest, agreement with the numerical calculation at  $U = 0$  is simply a modest check of our code. A more interesting limit is the computation of energies and energy gap at half-filling and large  $U$ . If we ignore the hopping term by comparison with the potential then the energy of the ground state at the classical level is zero (each site occupied by a single electron), and the energy of the first excited state is simply  $U$ , corresponding to having one doubly-occupied site. The actual values for the  $\varepsilon_i$  at  $f = 1$  and  $U = 30$  are shown in Fig. 8. The last occupied state on this  $24^2$  lattice is at state number  $M = 24^2 = 576$ , and the energy gap in this case is found to be  $\Delta\varepsilon = 24.6$ , which is not so far from  $U = 30$ . The energy density of the ground state is very nearly zero, due to a near-exact cancellation of the positive and negative energies of the occupied states. The convergence to  $\mathcal{E} = 0$  at half-filling with increasing  $U$ , and the near linear increase of  $\Delta\varepsilon$  with  $U$  for  $U > 4$  is seen in Fig. 9.

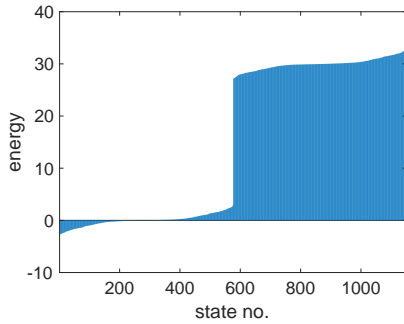


FIG. 8. One particle energies at  $U = 30$ ,  $f = 1$ . The energy gap between the last occupied and first unoccupied states is  $\Delta\varepsilon = 24.6$ .

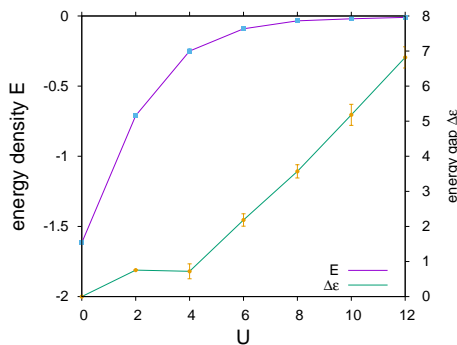


FIG. 9. Convergence to  $\mathcal{E} = 0$ , and linear growth of the energy gap  $\Delta\varepsilon$  with increasing  $U$ , at half-filling.

Subsequent figures will display the results (spin distribution, IPR values, etc.) taken from “typical” self-consistent so-

lutions of the Hartree-Fock equations although, as seen above and also in the next section, “typical” solutions can vary a great deal in certain observables, spatial ordering in particular.

### D. Spatial patterns in the spin distribution

Examination of the spatial distribution of charge and spin densities,  $C(x)$  and  $D(x)$  respectively in (18), reveal some interesting geometric patterns in the neighborhood of half-filling. The existence of stripes in Hartree-Fock treatments of the 2D Hubbard model goes back to [3–6], and there is also experimental evidence of stripe order in strongly correlated materials [17, 18]. We will focus here on the spin densities  $D(x)$ , which are displayed in Fig. 10 on a  $24^2$  lattice at  $U/t = 3$  at zero temperature near half filling.

At exactly half-filling one observes an antiferromagnetic “checkerboard” pattern, as seen in Fig. 10(d). Despite this apparently antiferromagnetic order, one should refrain from the interpretation that each electron is localized at one lattice site, in a pattern of alternating up/down spins. In fact this is far from the case, as is best seen from an examination of the IPR of each  $\phi_i$  at  $U/t = 3$ ,  $f = 1$ , which is shown in Fig. 11. The great majority of these IPR values are  $\approx 0.0025$ , and we recall that  $\text{IPR}=1$  means that a particle is localized at a single lattice site, while  $\text{IPR}=1/L^2$ , which is  $0.0017$  on a  $24^2$  lattice, is complete delocalization. It is evident that almost all single electron states extend over the entire lattice, and the picture of electrons localized at sites in an up/down alternating pattern, as strongly suggested by the checkerboard pattern, is completely untenable. It is remarkable that such highly unlocalized electrons nonetheless contrive to produce such a regular geometric pattern.

Stripe order in the spin density observable is seen in Fig. 10(b) at  $f = 0.8$ . This type of pattern is observed in many of the self-consistent Hartree-Fock solutions generated by our iterative procedure with random initial conditions, at moderate couplings in the neighborhood of half-filling. But it is not the only pattern found. An equally common pattern is the periodic arrangement of quasi-rectangular domains, seen in Fig. 10(c), again at  $f = 0.8$ . We emphasize that these different patterns are obtained at the same coupling parameters and at the same zero temperature. This is simply another feature of the multiplicity of self-consistent Hartree-Fock solutions, as already discussed, and is again indicative of just how different these different solutions can be. The possibility of domain structures of this kind was suggested previously in [19].

A more quantitative measure of long range order in magnetization is the momentum space correlator  $S(k_x, k_y)$  defined in (20). In Fig. 12 we display this quantity for the stripe, domain, and checkerboard patterns, corresponding to Figs. 10(b), 10(c) and 10(d), respectively, again at  $U = 3$  on a  $24^2$  lattice. Concentration of  $S(k_x, k_y)$  at just a few values (even just one  $k_x = k_y = \pi$  for the checkerboard pattern) is obviously evidence of long range order, and it is of interest to study the  $U$ -dependence. So let us choose  $f = 0.8$ , where we see both stripes and rectangular domains, and let  $S_4$  be the sum of the

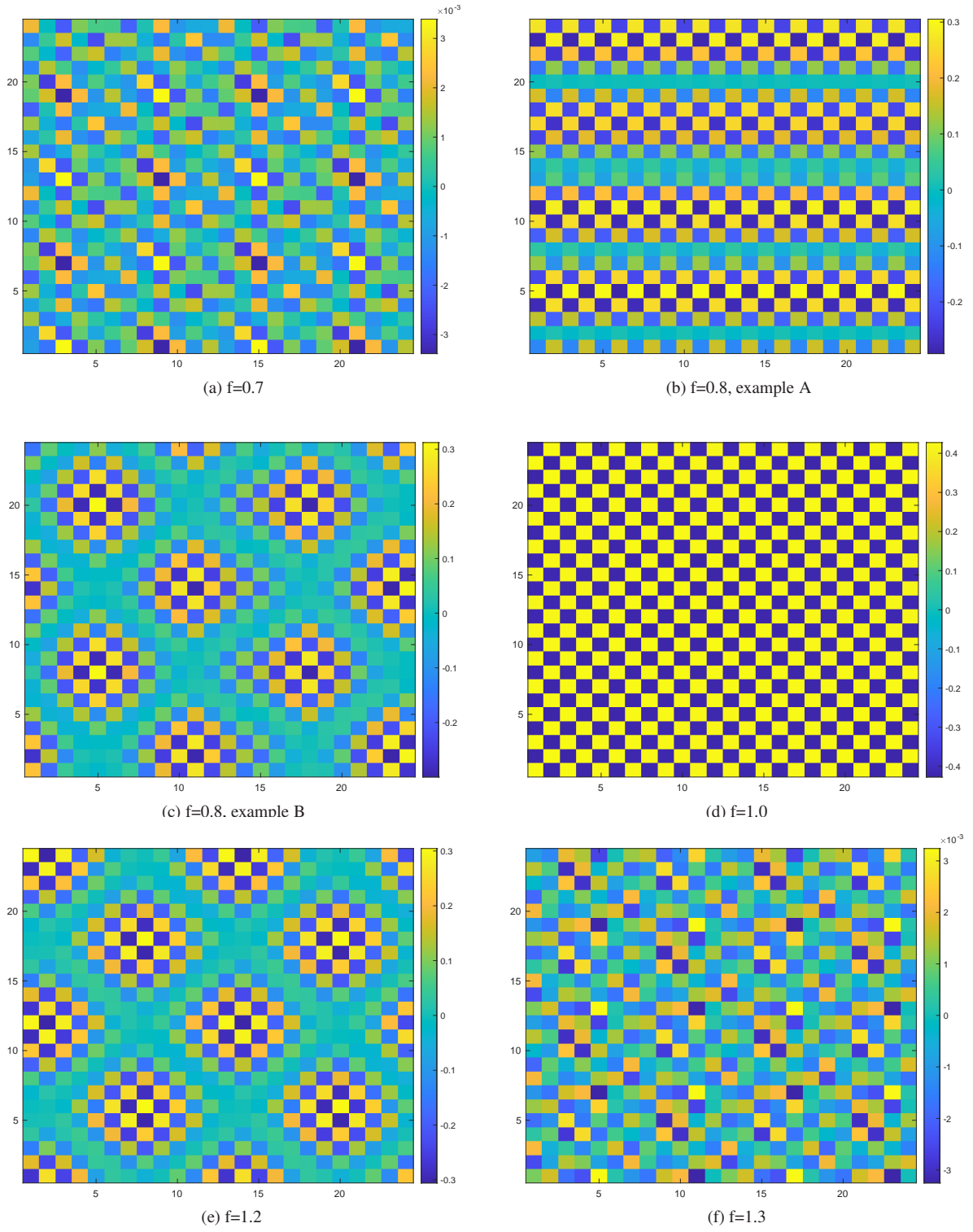


FIG. 10. Display of  $D(x)$  at filling fractions  $f = 0.7$  to  $f = 1.3$  and  $U/t = 3$ . The checkerboard pattern at  $f = 1$  (d) indicates an antiferromagnetic order across the  $24^2$  lattice area. Within the antiferromagnetic region, e.g. at  $f = 0.8$  and  $f = 1.2$ , both “wavelike” in (b) and “domains” shown in (c) and (e) are found, depending on the initialization. Outside the antiferromagnetic region there is no obvious pattern, and also the magnitude of  $D(x)$  (note the colorbar scale at (a) and (f)) is reduced by two orders of magnitude.

largest four values of  $S(k_x, k_y)$ , with  $S_{tot}$  the sum of all values. In Fig. 13 we plot the ratio  $S_4/S_{tot}$  (scale on the left-hand y-

axis), and  $S_4$  alone (scale on the right-hand y-axis). The long range order at  $U = 3$  decays away on either side. In addition,



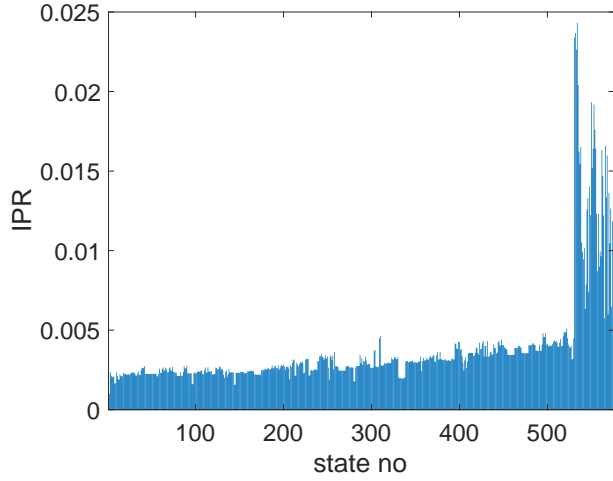


FIG. 11. Localization (IPR values) of one particle energy eigenstates  $\phi_i$  vs.  $i$  at  $U/t = 3, f = 1, 24^2$  lattice. Despite the checkerboard pattern seen at these values in Fig. 10, the one particle wavefunctions are either not at all, or only very weakly localized. Localization is a feature of strong repulsion (see Fig. 15 below), and is not associated with the stripe, domain, or checkerboard spatial patterns seen at moderate repulsion.

for  $U < 2$ ,  $S_4$  is hardly distinguishable from zero on the scale of the plot.

### E. Pair correlation and the checkerboard

It is obvious that in an eigenstate of particle number,  $\langle c(k, \uparrow)c(-k, \downarrow) \rangle = 0$ . On the other hand, the correlator of a pair creation operator in the vicinity of point  $x$ , and a pair destruction operator in the vicinity of point  $y$ , where  $R = |x - y| \gg 1$ , could be non-zero. Transforming to momentum space, as in eq. (25), it is of special interest to see where in  $k$ -space this operator is non-zero, and whether there is any indication of d-wave symmetry. In the ground state we find

$$\begin{aligned} \Delta(k', k) &= \langle \Phi | c^\dagger(k', \uparrow) c^\dagger(-k', \downarrow) c(k, \uparrow) c(-k, \downarrow) | \Phi \rangle \\ &= \sum_{j=2}^M \sum_{i=1}^{j-1} \{ \phi_i(-k', \uparrow) \phi_j(k', \downarrow) - \phi_i(k', \downarrow) \phi_j(-k', \uparrow) \} \\ &\quad \times \{ \phi_i(k, \uparrow) \phi_j(-k, \downarrow) - \phi_i(-k, \downarrow) \phi_j(k, \uparrow) \}. \end{aligned} \quad (27)$$

Define

$$\begin{aligned} \omega_{ij}(k) &= \phi_i(k, \uparrow) \phi_j(-k, \downarrow) - \phi_i(-k, \downarrow) \phi_j(k, \uparrow) \\ &= \phi_i(k, \uparrow) \phi_j^*(k, \downarrow) - \phi_i^*(k, \downarrow) \phi_j(k, \uparrow). \end{aligned} \quad (28)$$

Then

$$\Delta(k', k) = \sum_{j=2}^M \sum_{i=1}^{j-1} \omega_{ij}^*(k') \omega_{ij}(k). \quad (29)$$

The space of all  $k, k'$  is four-dimensional, and we choose a two dimensional slice by taking  $k'$  to be the wavevector  $k$  with  $x, y$  components interchanged, i.e  $k = (k_x, k_y), k' = (k_y, k_x)$ . If

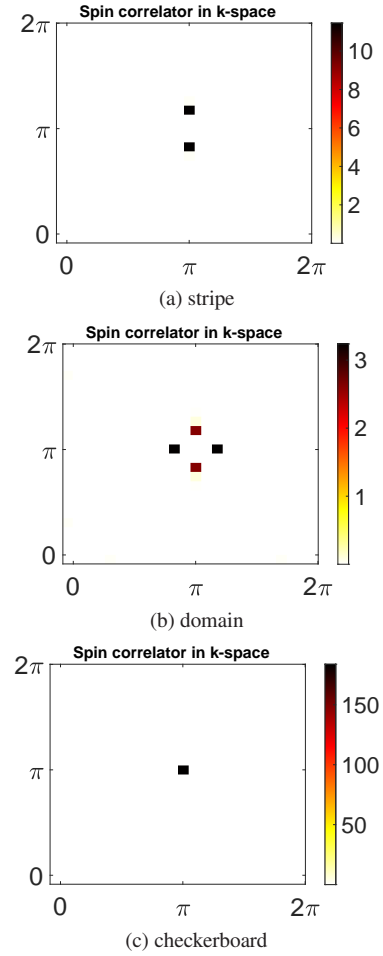


FIG. 12. Varieties of long-range order in momentum space as displayed by the momentum space spin correlator  $S(k)$ , defined in eq. (20), on a  $24^2$  lattice at  $U = 3$ . (a) stripe pattern,  $f = 0.8$ . (b) domain pattern, also at  $f = 0.8$ . (c) checkerboard pattern,  $f = 1$ .

pairing follows a D-wave pattern, then in this two-dimensional slice we would expect something like

$$\Delta(k', k) \sim -(\cos(k_x) - \cos(k_y))^2, \quad (30)$$

which is negative everywhere, and most negative at  $k_x = 0, k_y = \pm\pi$  and  $k_x = \pm\pi, k_y = 0$ .

These features are seen, roughly, but *only* for checkerboard patterns with the momentum space distribution shown in Fig. 14(a), in the immediate neighborhood of  $f = 1$ . The correlation is also only significant at the edge of the  $n(k)$  occupation zone. An example at  $f = 1, U/t = 1$  is shown in Fig. 14(a), but the very same correlation appears at half-filling over a range of two orders of magnitude, from  $U/t = 0.1$  to  $U/t = 10$ , and the corresponding plots are very similar to Fig. 14(a).<sup>2</sup>

The pair correlation at half-filling only starts to disintegrate below  $U/t = 0.03$ . The situation is quite different away from

<sup>2</sup> We are only interested in the correlator for  $k' \neq k$ , and have (arbitrarily) set  $\Delta(k, k) = 0$  in the figures shown.

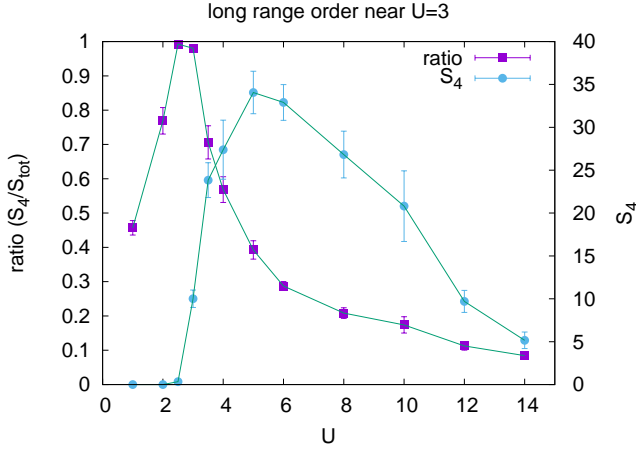


FIG. 13. A plot of  $S_4/S_{tot}$  (purple squares, left hand y-axis), and  $S_4$  alone (filled circles, right hand y-axis) vs.  $U$  at filling fraction  $f = 0.8$ . Here  $S_{tot}$  is the sum of all  $S(k)$  values, and  $S_4$  is the sum of the four largest  $k$  values. Long range order seems most evident near  $U = 3$ , where the sum is almost saturated by the top four values.

half-filling, e.g. the checkerboard order and similar pair correlation at  $f = 0.95$  is only seen at a rather strong repulsion of  $U/t = 10$  (Fig. 14(b)). The picture seen in Figs. 14(a) and 14(b) is not exactly what we have in eq. (30); for one thing the correlation is sharply concentrated at the boundary of the  $n(k)$  occupation zone, and the numerical values do not really agree with (30). But the fact that the correlator is everywhere negative, and most negative at  $(0, \pm\pi)$  and  $(\pm\pi, 0)$  is definitely reminiscent of d-wave correlation. We emphasize, however, that the checkerboard pattern and this type of pair correlation are only found in the immediate neighborhood of half-filling, and even then (e.g. at  $f = 0.95$ ) may only be seen at comparatively large values of  $U/t$ , as in Fig. 14(b). When the checkerboard pattern is absent the correlation function  $\Delta(k, k')$  is still generally concentrated at the edge of the  $n(k)$  distribution, but may be everywhere positive, or a mixture of positive and negative values. Or the pair correlation may be negligible, as seen in Fig. 14(c) (note the scale) at  $f = 0.8, U = 3$ , where there is a stripe order.<sup>3</sup>

### F. Localization and particle-hole symmetry

The stripe, domain and checkerboard patterns do not imply that one electron wave functions are localized, and in fact the opposite is true, as we have already noted. It is expected that one particle wavefunctions ought to be localized at sufficiently strong  $U/t$ , and this can be seen in Fig. 15, at filling fractions  $f = 0.9, 1.0, 1.1$  and  $U/t = 30, 100$ . In this figure we display the IPR values of all  $2L^2$  particle states ( $L = 24$ ), both filled and unfilled. An interesting feature is that it is the hole

<sup>3</sup> We note that a weak-coupling analysis of the 2D Hubbard model in ref. [20] also found d-wave pairing strongest near half-filling.

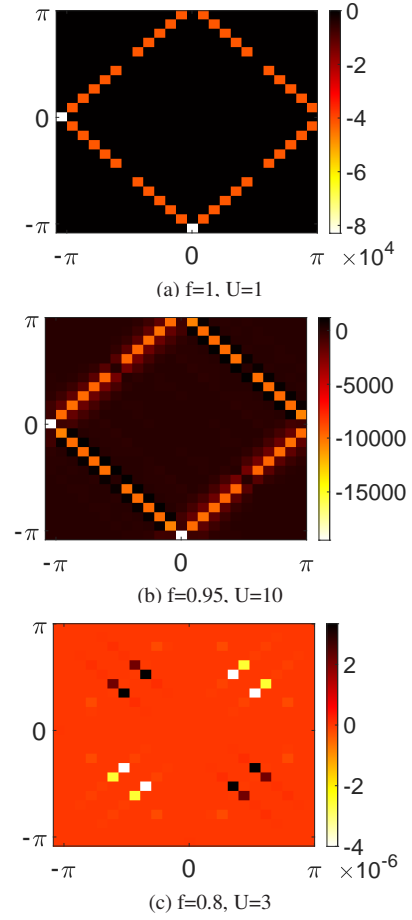


FIG. 14. Display of the pair correlation function  $\Delta(k', k)$  in the  $k_x, k_y$  plane, where  $k' = (k_x, k_y), k = (k_y, k_x)$ . (a) The pattern shown, at half-filling and  $U = 1$ , has some of the features of d-wave correlation. This pattern is virtually unchanged at half-filling across two orders of magnitude, from  $U = 0.1$  to 10. (b) Pair correlation at  $f = 0.95$  and  $U = 10$ . Even slightly away from half-filling, the pattern seen here at  $U = 10$  is not seen at moderate and small values of  $U$ . (c) The correlator is negligible (note the scale), compared to the previous subfigures, at  $f = 0.8, U = 3$ . The pattern seen in (a) and (b) is always associated with a checkerboard pattern, and in case (c) there is instead a stripe pattern.

(unfilled) states which are localized at  $f < 1$ , and the electron (filled) states which are localized at  $f > 1$ , with about an equal degree of localization among hole and particle states at  $f = 1$ . The dramatic shift from localized holes at  $f < 1$  to localized electrons at  $f > 1$ , no doubt a consequence of particle-hole symmetry, is most obvious at an extremely strong coupling  $U/t = 100$ , but it is also quite evident at, e.g.,  $U/t = 30$ . As  $U/t$  further reduced to moderate values, the asymmetry in particle/hole localization on either side of  $f = 1$ , and the localization itself, gradually disappears.

Anderson localization is a well known phenomenon for particle propagation in a random potential, and it is perhaps significant that we here have, by contrast, localization in a translationally invariant system, where the degree of localization among the different states depends on the random initializa-

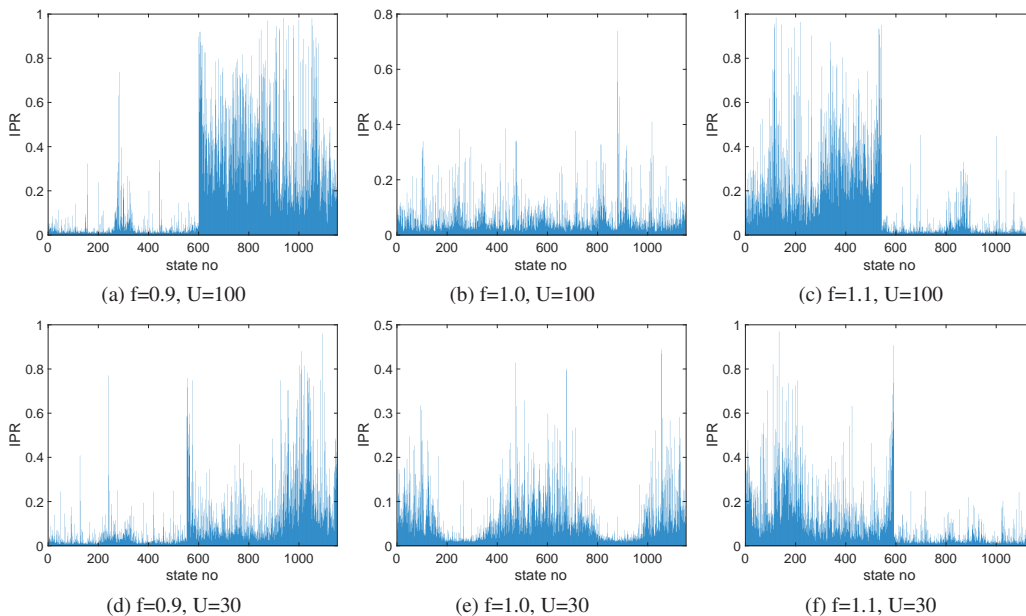


FIG. 15. Localization of particle and hole one-particle states at very strong repulsion  $U = 30, 100$  as quantified by their IPR values. The  $x$ -axis is the one-particle state number, i.e. the  $i$  of  $\phi_i(x, s)$ . Note that it is hole states which are localized for  $f < 1$ , and particles states which are localized for  $f > 1$ , with a symmetric distribution at  $f = 1$ . Subfigures (a,b,c):  $U = 100$  and  $f = 0.9, 1.0, 1.1$  respectively. Subfigures (d,e,f):  $U = 30$  and  $f = 0.9, 1.0, 1.1$  respectively.

tion. This seems to answer in the affirmative the question raised in [21], which asks whether this phenomenon is possible.

## V. CONCLUSIONS

The Hartree-Fock approach yields a multiplicity of self-consistent solutions of surprising complexity; more complexity than one might expect from a single Slater determinant, where entanglement is limited to what is required by Fermi statistics. We see emergent spin patterns in the form of stripes, checkerboards, and rectangular domains, band gaps correlated with antiferromagnetic order, localization of particles or holes for strong repulsion at  $f > 1$ ,  $f < 1$  respectively, and pair correlation functions near half-filling which have properties similar to d-wave distributions. Perhaps most important is the multiplicity itself; i.e. the enormous number self-consistent solutions of the Hartree-Fock equations, derived from an iterative procedure with only slightly different random initializations, that are very nearly degenerate in energy.

One can take different views of this near degeneracy. One view is that the true ground state, so far as it can be determined in the Hartree-Fock approach, is the state with the lowest energy. This is in a landscape of states which have very nearly the same energy, but are distinguished from one another by other observables, such as local magnetization and energy gap, which can differ widely among different solutions. In our opinion this view is much like asserting that there is one “true” lowest energy ground state of a spin glass, despite the fact that the system very rarely finds its way to that state. The

other possible view, if we take the multiplicity of near degenerate states seriously, is that the 2D Hubbard model may in fact have certain features analogous to spin glasses, e.g. some degree of non-ergodicity, which deserve further study.

We have also found localization of one-particle hole and electron states just below and just above half-filling, at strong repulsion, with IPR values which again depend on the particular solution obtained from the particular initialization. This is not Anderson localization, of course, because the Hubbard Hamiltonian is intrinsically translation invariant. There has been speculation [21] whether small random differences in initialization might drive a system to become localized, and our results would seem to support that possibility.

The Hartree-Fock approach to the Hubbard model must obviously be viewed with caution; we are not aware of any method which would systematically improve the results or quantify their error. On the other hand, in its defense, we have seen that apart from very strong repulsion, the one-electron wave functions are unlocalized. That means that a single electron is effectively interacting with all other electrons in the system, and not just with a handful of nearest neighbors. The fact that one degree of freedom is interacting with many is the usual mean-field (and in particular Hartree-Fock) justification for replacement of the “many” by their average. But until a truly reliable method for dealing with the sign problem comes along, or perhaps an experimental realization of the Hubbard model via cold atoms, the validity of the Hartree-Fock approach to the 2D Hubbard model is hard to assess.

All of the work presented in this article concerns the zero temperature Hartree-Fock ground state (or states) of the 2D Hubbard model. We leave the effects of finite temperature to

later investigation.

ergy under Grant No. DE-SC0013682.

### ACKNOWLEDGMENTS

This research is supported by the U.S. Department of En-

- 
- [1] D. R. Penn, Phys. Rev. **142**, 350 (1966).  
 [2] J. E. Hirsch, Phys. Rev. B **31**, 4403 (1985).  
 [3] D. Poilblanc and T. M. Rice, Phys. Rev. B **39**, 9749 (1989).  
 [4] J. Zaanen and O. Gunnarsson, Phys. Rev. B **40**, 7391 (1989).  
 [5] K. Machida, Physica C: Superconductivity **158**, 192 (1989).  
 [6] H. Schulz, Journal de Physique **50**, 2833 (1989).  
 [7] M. Ichimura, M. Fujita, and K. Nakao, Journal of the Physical Society of Japan **61**, 2027 (1992), <https://doi.org/10.1143/JPSJ.61.2027>.  
 [8] M. Imada, A. Fujimori, and Y. Tokura, Rev. Mod. Phys. **70**, 1039 (1998).  
 [9] P. Fazekas, Lecture Notes on Electron Correlation and Magnetism (WORLD SCIENTIFIC, 1999), <https://www.worldscientific.com/doi/pdf/10.1142/2945>.  
 [10] J. Xu, C.-C. Chang, E. Walter, and S. Zhang, Journal of physics. Condensed matter : an Institute of Physics journal **23**, 505601 (2011).  
 [11] R. Rodríguez-Guzmán, C. A. Jiménez-Hoyos, R. Schutski, and G. E. Scuseria, Phys. Rev. B **87**, 235129 (2013).  
 [12] Simons Collaboration on the Many-Electron Problem, J. P. F. LeBlanc et al., Phys. Rev. X **5**, 041041 (2015).  
 [13] E. Pavarini, E. Koch, A. Lichtenstein, and D. Vollhardt, editors, The LDA+DMFT approach to strongly correlated materials, Schriften des Forschungszentrums Jülich. Reihe modeling and simulation Vol. 1 (Forschungszentrum Jülich GmbH Zentralbibliothek, Verlag, Jülich, 2011).  
 [14] C. N. Varney et al., Phys. Rev. B **80**, 075116 (2009).  
 [15] R. Blankenbecler, D. J. Scalapino, and R. L. Sugar, Phys. Rev. D **24**, 2278 (1981).  
 [16] J. Kertesz, Physica **A161**, 58 (1989).  
 [17] S. A. Kivelson et al., Rev. Mod. Phys. **75**, 1201 (2003).  
 [18] J. M. Tranquada, Symmetry **13**, 2365 (2021).  
 [19] B. V. Fine, Phys. Rev. B **70**, 224508 (2004).  
 [20] S. Raghu, S. A. Kivelson, and D. J. Scalapino, Phys. Rev. B **81**, 224505 (2010).  
 [21] R. Nandkishore and D. A. Huse, Annual Review of Condensed Matter Physics **6**, 15 (2015).